NASA Technical Memorandum 104427

Experiments With Phase Change Thermal Energy Storage Canisters for Space Station Freedom

Thomas W. Kerslake
Lewis Research Center
Cleveland, Ohio

NASA

EXPERIMENTS WITH PHASE CHANGE THERMAL ENERGY STORAGE CANISTERS

FOR SPACE STATION FREEDOM

Thomas W. Kerslake[*]
National Aeronautics and Space Administration
Lewis Research Center
Cleveland, Ohio 44135

ABSTRACT

The solar dynamic power module proposed for the growth Space Station Freedom uses the heat of fusion of a phase change material (PCM) to efficiently store thermal energy for use during eclipse periods. The PCM, a LiF-20CaF$_2$ salt, is contained in annular, metal canisters located in a heat receiver at the focus of a solar concentrator. This paper discusses PCM canister ground-based experiments and analytical heat transfer studies. The hardware, test procedures, and test results from these experiments are discussed. After more than 900 simulated Space Station Freedom orbital cycles, no canister cracks or leaks were observed and all data were successfully collected. The effect of 1-g test orientation on canister wall temperatures was generally small while void position was strongly dependent on test orientation and canister cooling. In one test orientation, alternating wall temperature data were measured that supports an earlier theory of oscillating vortex flow in the PCM melt. Analytical canister wall temperatures compared very favorably with experimental temperature data. This illustrates that ground-based canister thermal performance can be predicted well by analyses that employ straight-forward, engineering models of void behavior and liquid PCM free convection. Because of the accuracy of analytical models and the relative insensitivity of 1-g performance to test orientation, canister performance in micro-g should be predictable with a high degree of confidence by removing gravity effects from the analytical modeling.

1 INTRODUCTION

Conventional photovoltaic solar power systems operating in low earth orbit use electrochemical batteries to store energy for use during eclipse periods. The solar dynamic power module proposed for the growth Space Station Freedom, however, uses the heat of fusion of a phase change material (PCM) to more efficiently store thermal energy for eclipse periods. The PCM, a LiF-20CaF$_2$ salt, is contained in annular, metal canisters located in a heat receiver [1], shown in figure 1, which accepts focussed solar energy from a parabolic concentrator. Due to the cyclic PCM freeze-thaw behavior, the canisters remain near the PCM melting point, 1042 K, and are thus able to continuously heat a working fluid circulating through the heat receiver during an entire orbit. The hot working fluid, in turn, drives a turbo-alternator to produce electric power.

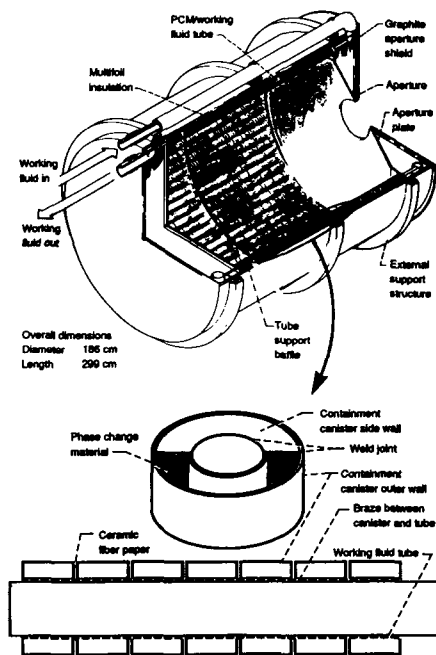[*]Aerospace Engineer, Associate Member ASME.

Figure 1.—Heat receiver.

To effectively design the heat receiver and canisters, the nature of PCM heat transfer during orbital, micro-g operation must be characterized. PCM heat transfer in 1-g is also important since flight hardware will likely be verified with ground-based test data. Differences in heat transfer performance between micro-g and 1-g environments are expected as a result of two factors: (1) liquid PCM convection and (2) PCM void position within the canister. (A 20 to 25 percent void volume is created within a canister due to PCM solidification shrinkage.) In 1-g, buoyant forces create liquid PCM circulation and tend to place the void generally at the canister top. In micro-g, surface-tension driven liquid PCM flows are small (or nonexistent) and the void will generally reside at the hottest region of the canister during solidification, [2]-[3]. However, the effect of these different gravity environments on PCM canister heat transfer has not been quantified.

In this report, the issue of gravity dependency is addressed by examining results from experimental and analytical PCM canister heat transfer studies. The hardware, test procedures, and test results from ground-based canister experiments in various orientations are discussed. Experimental canister wall temperature data are correlated with numerical predictions from a previously developed computer program which models ground-based canister heat transfer. Wall temperatures are an important measure of performance since they determine heat transfer to the working fluid, receiver cavity infrared radiation exchange, and long-term canister material durability. Using these experimental data and the complementary numerical predictions, the quantitative accuracy of the canister computer model is determined. Ground test orientations for future PCM canister and receiver tests are also recommended.

2 EXPERIMENTS

2.1 Test Articles

Three test PCM canisters were fabricated and provided to Lewis Research Center by Allied-Signal Aerospace Company, AiResearch Los Angeles Division. Each of the three canisters was bead-blasted to roughen exterior surfaces and instrumented with nine type K (chromel-alumel), high accuracy (±3/8 percent) thermocouples on the outer wall and on one side wall. The physical characteristics of these test canisters, whose dimensions and PCM masses are slightly different from those given in [1] for flight canisters, are given in table I. The position and numbering convention for the thermocouples are shown in figure 2. Thermocouple 1 was attached to the region of the canister outer wall that consistently faced the radiant heat source for all tests. Two additional thermocouples, numbered 10 and 11, were installed on the outer wall of canister B. These thermocouples were located

2

+ 45° and -45° around the canister circumference from the position of thermocouple 1 (figure 2). The additional thermocouples were added in an attempt to measure wall temperature fluctuations induced by oscillating free convective flow vortices in the PCM melt, [4] and [5].

TABLE I. TEST CANISTER DESIGN FEATURES

Material of construction	Haynes alloy 188
Outer Diameter/Wall Thickness	4.98 cm/0.129 cm
Inner Diameter[a]/Wall Thickness[b]	2.07 cm/0.261 cm
Length/Side Wall Thickness	2.43 cm/0.091 cm
Phase Change Material (PCM)	$LiF-20CaF_2$
PCM Melting Point	1042 K
PCM Heat of Fusion	816 J/g
PCM Mass	53 g
Total Canister Mass	137 g

[a]Cooling air tube.
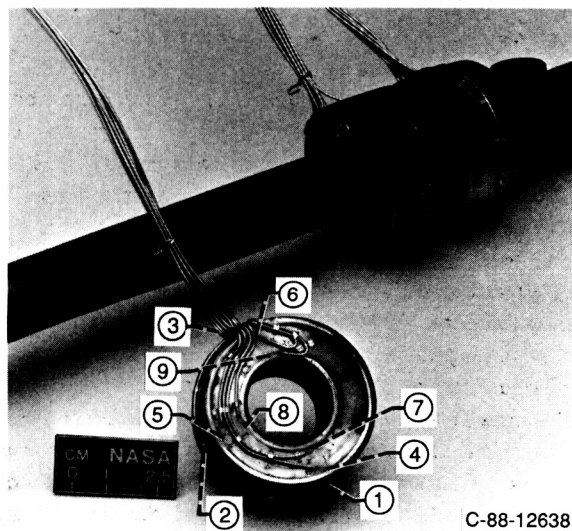[b]Thickness of canister inner wall plus cooling air tube wall.

Figure 2.—Canister thermocouple instrumentation.

The three test canisters, denoted A, B, and C, were slip-fit side-by-side over a Haynes Alloy 188 (HA 188) cooling air tube. With respect to the direction of cooling air flow, canisters A, B, and C were consistently located up-stream, mid-stream, and down-stream, respectively, for all tests. Refractory fiber, blanket insulation was wrapped around the cooling air tube and also placed between adjacent canisters to simulate canisters on a portion of a flight receiver tube, [1]. The tube was then inserted into the insulated test chamber shown in figure 3.
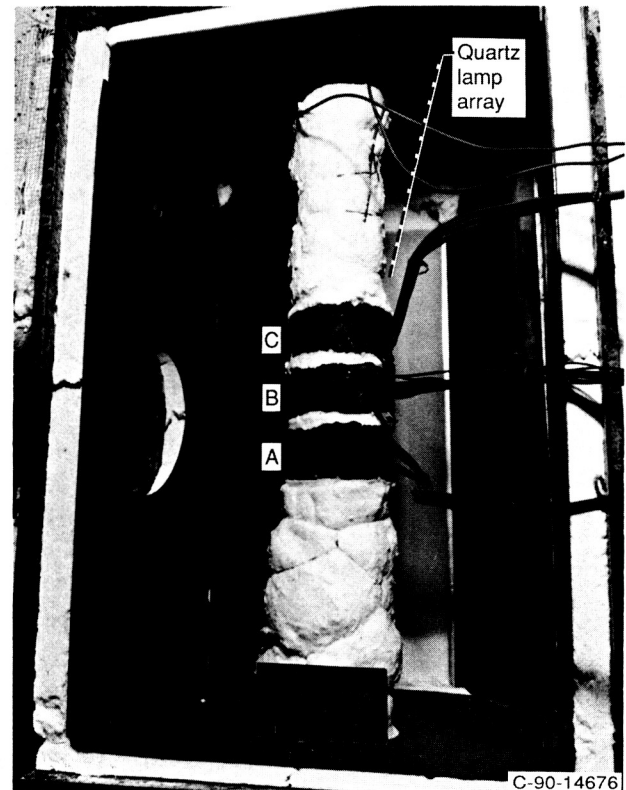

Figure 3.—Canisters installed in test chamber.

2.2 Test Apparatus

Figure 4 shows a photograph of the test apparatus. The primary hardware elements of this apparatus included an insulated test chamber, a quartz lamp array radiant heater, and an air preheater. The test chamber consisted of a steel box insulated with several layers of refractory board insulation with the radiant heater comprising one chamber surface (figure 3). Visible from the outside of the chamber were tube penetrations for the preheated
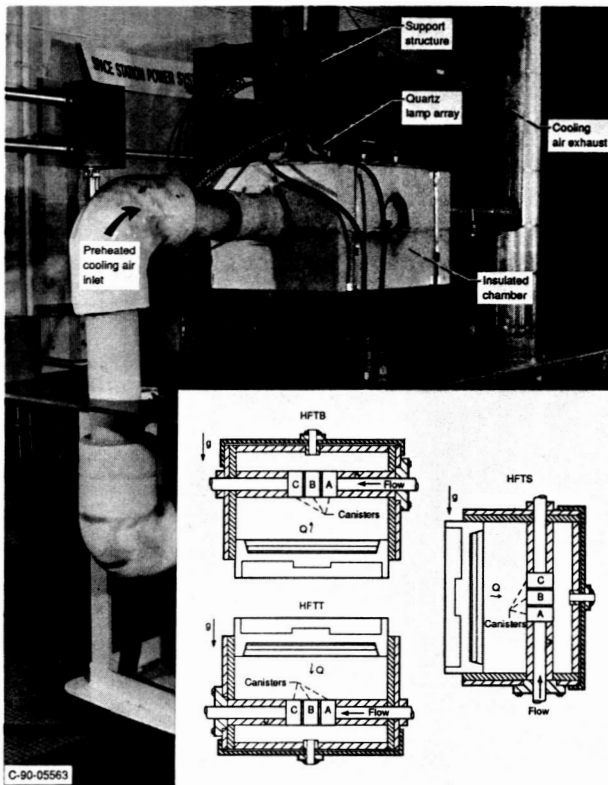
Figure 4.—Canister test hardware and test orientations.

cooling air inlet and exhaust (figure 4). The other interior walls of the chamber were lined with pre-oxidized, bead-blasted HA 188 sheet with known optical surface properties that matched those of the canisters. The HA 188 sheet pieces were instrumented with type K thermocouples. The positions of the chamber lid and radiant heater surface were both adjustable. This allowed tailoring of the canister absorbed flux distribution by changing the chamber geometry. In addition, the chamber support structure could be reconfigured to achieve three different test orientations: (1) Heat From The Bottom (HFTB), (2) Heat From The Top (HFTT), and (3) Heat From The Side (HFTS). In all of these test orientations, shown in figure 4, radiant heat was applied to the canister outer peripheral surfaces only.

The radiant heater consisted of six parallel, 2-kWe linear quartz lamps in a water-cooled, aluminum housing cov-

ered by a frosted, quartz plate. Heat flux measurements at and above the plate were made using a calibrated foil calorimeter. Using these measurements, the relationship between applied lamp electrical power and the heat flux produced at the plate surface could be determined. The measurements also confirmed that the quartz plate closely approximated a uniform, diffuse heat source. Electrical power to the lamps was regulated by a solid-state power supply.

The air preheater consisted of three electrical resistance tube heaters plumbed in series upstream of the chamber cooling air inlet. Electric power to the air preheater was regulated by a solid-state power supply. Cooling air was supplied by a facility source at 862 kPa gauge and 289 K. Air flow rate was measured by a calibrated orifice-type flow meter and held nominally constant at 40.8 kg/hr for all tests by manually adjusting a valve.

Other important elements (not shown in figure 4) included a two-channel, programmable controller and an ESCORT II data acquisition system. The controller executed two separate programs to control the electric power supply output levels to the radiant heater and air preheater based on power and air temperature (measured at the tube inlet to the chamber) feed back signals, respectively. Therefore, the transient, cyclic absorbed flux and coolant temperature profiles for any canister of interest in the receiver could be simulated. For these tests, the profiles of canisters under the greatest thermal loading in the receiver, i.e., those located 84 cm down the tube from the receiver aperture end, were simulated (figure 1). Limit switches could de-energize the SCR's if an unsafe condition occurred, thereby allowing continuous, unattended operation.

The Lewis Research Center ESCORT II data acquisition system was configured to: measure raw data, convert the data

4

to engineering units, perform basic data reduction, store the data, provide warnings or alarms if preset parameter limits are exceeded, and present data in real-time on television monitors in the test facility control room. Measured data included air flow meter pressure drop, radiant heater and air preheater electrical power levels, and temperatures of the canisters, test chamber interior walls, inlet cooling air, and the ambient. Final data reduction, performed on a VAX 8800 computer, calculated absorbed canister fluxes (see section 3.2) and produced tabular and graphical data output.

2.3 Test Procedures

Initial cyclic tests, in the HFTB orientation, were performed with various chamber lid and radiant heater surface positions. After several iterations, the chamber geometry that resulted in the desired canister absorbed flux distribution was obtained: that is, approximately 70 percent of the energy was absorbed on half the canister peripheral surface viewing the radiant heater while 30 percent was absorbed on the other half. This distribution corresponds with the ratio of projected canister surface area to projected receiver tube spacing area given in [1]. The resultant spacings from the canister outer diameter to the chamber lid and to the radiant heater surface are 2.8 cm and 14.0 cm, respectively. These spacings were held fixed throughout the testing.

A series of tests was conducted in the following order: 500 cycle HFTB, 100 cycle HFTB, 100 cycle HFTT, 100 cycle HFTS (with the instrumented canister side wall down), and 100 cycle HFTS (with the instrumented canister side wall up). Each cycle has a 91.1 min period of which 54.7 min simulates orbital insolation and 36.4 min simulates orbital eclipse. In each test orientation, steady state tests were initially conducted in which radiant heater power and cooling air inlet

temperature values were held constant. These data were used to select appropriate radiant heater power levels for the subsequent 100 cycle test and to determine heat losses. Prior to the start of each cyclic test, the test chamber and canisters were stabilized at a nominal 922 K temperature for a 12 hr period.

The 500 cycle test was performed initially to determine potential long-term canister performance changes associated with unstable PCM properties and/or unstable HA 188 optical properties. This test showed that canister temperature data were stable and repeatable after 100 cycles and thus, longer tests were unnecessary to obtain repeatable thermal performance data. (In addition, long-term tests were in progress elsewhere, [6].) Furthermore, subsequent 100 cycle tests demonstrated data repeatability after only 10 cycles. This probably indicates that the HA 188 surfaces formed a sufficiently thick oxide layer during the 500 cycle test to mitigate any further changes in surface optical properties.

The last test conducted was a repeat of the 100 cycle HFTS test, but with the canisters remounted on the cooling air tube with the instrumented side walls on top. This test was conducted to determine the difference in temperatures between the canister bottom side wall (adjacent to PCM) and top side wall (adjacent to PCM void). In the other test orientations, near longitudinal symmetry exists so that both canister side walls operate at essentially the same temperature.

2.4 Radiography

Before and after tests in each orientation, x-ray radiographs of the three canisters were taken (at room temperature) by a Muller MG 150 x-ray machine. Five images of each canister were produced using A and T film: four longitudinal cross sections (showing (r,z) detail) and one axial cross section

(showing (r,θ) detail). Solid PCM distributions within canisters were clearly revealed by the radiographs. Features of the canister electron-beam weld joints were also visible. With the x-ray source operating at 140 to 160 keV and 4 mA, exposure periods of 4 to 7 min were required to obtain an image. Hence, the possibility of producing images of the transient PCM freeze-thaw processes during a canister test, as was done in [7], was ruled out due to the long exposure periods required.

## 3 ANALYSIS

3.1 Canister Heat Transfer

A numerical analysis was performed to predict the thermal performance of canister B during the tenth cycle of the first HFTS test. The computer program "NUCAM-2DV" (described in [3], [8], and [9]) was used for this analysis. This program employed a simple-explicit, finite-difference numerical technique to analyze a two-dimensional, axisymmetric PCM canister geometry. Phase-change heat transfer was modeled using the "enthalpy method", where specific enthalpy, e, was determined through the conservation of energy equation:

$$\frac{\partial(\rho e)}{\partial t} = \text{div}[k\vec{\nabla}T] \ , \qquad (3.1)$$

where ρ, k, and T are the PCM density, conductivity, and temperature, respectively. PCM temperature and phase distributions were then related to specific enthalpy by a set of constitutive equations. A constant volume, fixed location void model that calculates radiation and PCM vapor conduction heat transfer was included. Liquid PCM free convection was modeled through the use of a liquid conductivity multiplier based on existing empirical Nusselt number correlations.

Two modifications were made to this computer program to better model the

physical characteristics of the test canister. First, the PCM void was moved from a location adjacent to the outer wall to one adjacent to the canister top side wall (figure 5). This location was consistent with radiographic canister observations for this test orientation. Second, an additional term was included in the overall heat transfer coefficient between the canister inner wall and cooling air flow. This accounted for the 0.002 to 0.005 cm air gap that existed between the slip-fit canister and cooling air tube.
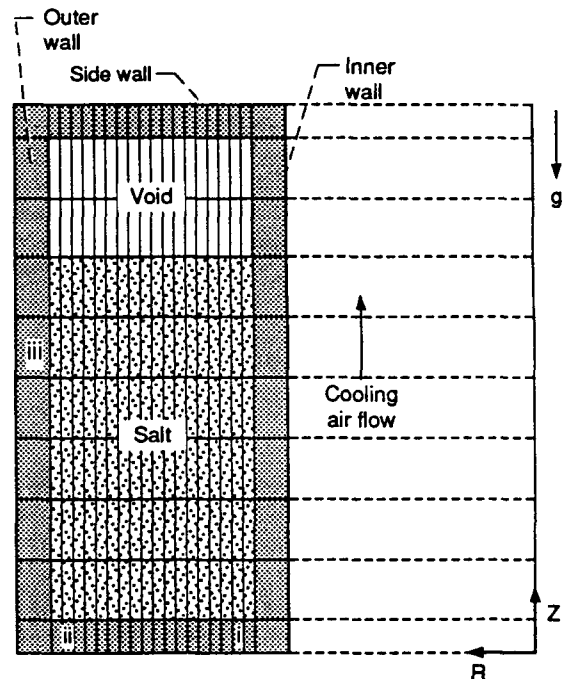
i – Element (3, 1) ii – Element (18, 1) iii – Element (20, 6)

Figure 5.—Canister finite-difference element model.

3.2 Test Chamber Heat Transfer

To calculate canister thermal loadings, the net-absorbed heat flux at the canister outer peripheral surface must be determined. Therefore, the test chamber radiation heat transfer must be analyzed. For this analysis, the assumptions of opaque, gray, diffuse chamber surfaces and a uniform, diffuse heat source were invoked. In addition, it was assumed that the air in the test chamber behaved as a nonparticipating medium. Thus, from enclosure radiation

6

theory ([10]), the net radiative heat losses for surfaces in the enclosure, Q_j/A_j, were determined by the equation set:

$$\sum_{j=1}^{N}\left\{\frac{\Delta_{kj}}{\varepsilon_j} - \left(\frac{1-\varepsilon_j}{\varepsilon_j}\right)F_{kj}\right\}\frac{Q_j}{A_j} = \sum_{j=1}^{N} F_{kj}\sigma(T_k^4 - T_j^4).$$ (3.2)

where k indexes from 1 to N. The subscripts k and j are chamber surface element numbers that take on all integer values between 1 and N, the total number of elements. The term Δ_{kj} is the Kronecker delta equal to 1 for k=j and equal to 0 for k≠j. The term σ is the Stefan-Boltzmann constant and ε_j is the surface element emittance. For surface elements 1 through N-1, T_j was specified based on thermocouple data. For the Nth surface element, representing the radiant heater, the net heat flux, Q_N/A_N, was specified as a function of applied electrical power. Element-to-element view factors, F_{kj}, were calculated using the commercially available computer program TRASYS (Thermal Radiation Analysis System).

This system of equations was solved at discrete times throughout the cycle to determine the time-dependent, net absorbed heat flux for the canister front side (radiant heater facing) and back side (chamber lid facing). Using these heat flux terms, the radiant heater electrical power controller program could be set to achieve the desired cyclic absorbed flux profiles for the canisters. These flux values were also used as the outer wall boundary condition in the canister numerical analyses.

3.3 Heat Flux Correction

Preliminary calculations showed that the magnitude of free convection heat transfer between the canisters and the test chamber air would be less than 10

percent that of radiation heat transfer. These calculations assumed that the test chamber would act like a leak-tight, air furnace. In practice, however, the assembled chamber had significant leaks that allowed the exchange of cool ambient air. Hence, the radiative net-absorbed heat flux terms had to be corrected to account for convective heat exchange. This was accomplished by iteratively matching analytical temperature predictions with temperature data from the steady state HFTS tests. The heat flux correction factor was then defined as the difference between the analytical heat flux used (section 3.1) and the empirically derived heat flux (section 3.2). This procedure was repeated for several steady state test points to generate the functional relationship between the heat flux correction and canister outer wall temperature. The corrected heat flux profile was then used to analytically predict transient canister B performance for cycle 10 of the HFTS test orientation.

4 DISCUSSION OF RESULTS

4.1 Post-Test Condition Of Canisters After 900 Thermal Cycles

All canister surfaces had a tenacious, dull-black oxide coating which is characteristic of HA 188 after heat treating in air. No cracks at weld joints or in the parent material were observed visually or radiographically and there were no PCM leaks. Slight outward deformation (i.e., 0.05 to 0.13 cm) was visible in the outer wall and one side wall of canister A and in one side wall of canister B. In canister A, the outer wall deformation corresponded to the location of the canister seam weld. From radiographic inspection, it was known that this seam weld was poorly fused. Hence, localized stresses in this region were increased. The side wall deformation in both canisters A and B was located in the vicinity of thermocouples 4 and 7 (figure 2). This

region experienced the highest side wall temperatures during testing because it was closest to the radiant heater. This region was also near the canister bottom for 600 cycles of HFTB testing where PCM expansive forces during melting could be greatest.

Although this deformation is significant, it is not totally surprising since the canisters were not specifically designed or fabricated for this kind of testing. The canisters were originally built using existing materials for a low-cost, concept demonstration test and thus, had under-sized wall thicknesses and partially fused, uninspectable weld joints. (Current canister designs have fewer, fully inspectable weld joints and appropriate. wall thicknesses.) The canisters were then tested for an extended number of cycles using the latest, worst-case, receiver heat flux and temperature predictions. These predictions were more demanding than those at the time the canisters were fabricated. However, the tests were conducted based on the engineering judgement that obtaining the highest fidelity canister performance data outweighed the risk of canister structural damage. The fact that the canisters could withstand this deformation without failing illustrates the inherent structural robustness of the canister material, HA 188, and the electron-beam weld joints.

4.2 Test Thermal Boundary Conditions

Figure 6 shows the average (corrected) net-absorbed heat flux and cooling air inlet temperature for the canisters during cycle 10 of the HFTS test orientation. Note that the net-absorbed heat flux is negative for the entire eclipse simulation period. This has an important impact on PCM solidification patterns. Radiographs show that these heat losses create solid PCM formations around the outer canister wall in addition to the expected solid PCM formation around the air-cooled, inner wall (see section 4.3.2).
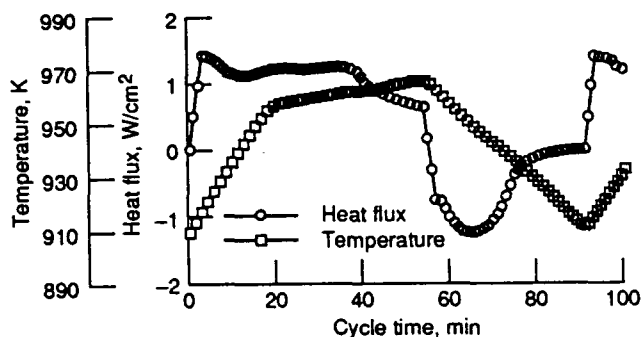

Figure 6.—Corrected average canister absorbed heat flux and cooling air inlet temperature for the HFTS test orientation, cycle 10.

4.3 Effect Of Test Orientation

4.3.1 Temperature Data. - The effect of test orientation on wall temperatures is seen in figure 7 which shows canister B, cycle 10 temperature data (thermocouples 1, 3, and 8) for the HFTB, HFTT, and HFTS test configurations. These data are also representative of those from canisters A and C. Independent of test orientation, all data measured by any one thermocouple exhibit similar values and transient characteristics (excluding the HFTT test to be discussed later). The difference between canister top and bottom side wall temperatures in the HFTS orientation is also small during the heating part of the cycle, i.e., less than ~10 K. However, during the cooling part of the cycle, temperature differences are up to 3 times larger. These larger differences are attributed to slower cooling of the bottom side wall, in contact with solidifying PCM, with respect to the top side wall adjacent to void space. In related tests in which the test orientation was held constant and the void distribution changed [11], very little difference in wall temperatures was measured as well. This indicates the relative insensitivity of canister wall temperatures to the gross void distributions for these test orientations.

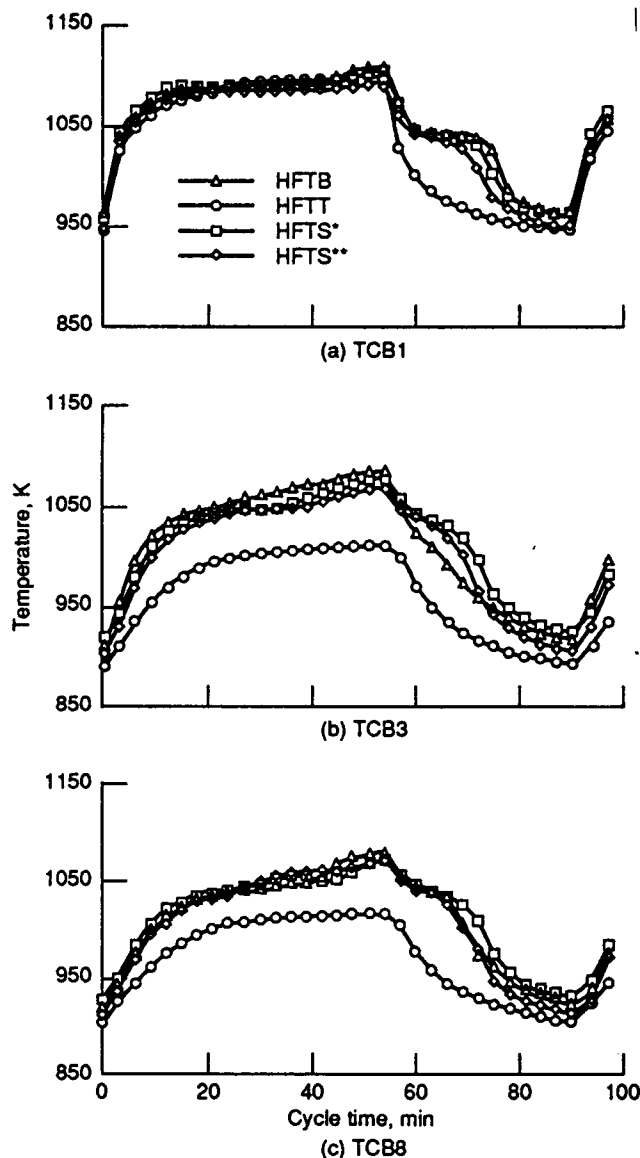The canister B temperature data are also consistent with pretest

8

Figure 7.—Midstream canister temperature data for cycle 10. (* = TC's down, ** = TC's up)

to a region of canister wall in contact with PCM as in figure 7(a), HFTB. However, thermal-arrest is not exhibited by the same thermocouple in the HFTT orientation data (figure 7(a)). Hence, it can be concluded that no PCM is in contact with the canister wall near the location of thermocouple 1. This is to be expected for the HFTT test orientation in which the void will generally be at the top. In addition, HFTT data in figure 7(b) and (c) show that the PCM melting temperature is not exceeded at other canister wall locations. Therefore, there is no cyclic PCM melting-freezing during the HFTT test.

There are two primary reasons for the lack of PCM melting during the HFTT test: (1) canisters are closer to probable leaks of cold ambient air into the bottom of the chamber and (2) the cold air leaks cool internal wall temperatures in the lower region of the chamber. These effects act to increase canister convective heat losses and reduce radiation heat transfer to the canister back sides (where most of the PCM is located). Hence, the amount of PCM that can melt is also reduced. This explanation is supported by test chamber radiation heat transfer calculations which show that for a given radiant heater flux, the canister back side net-absorbed heat flux is 36.7 percent lower in the HFTT orientation when compared to the HFTS orientation. Therefore, to eliminate this test chamber-related difficulty, future canister (and receiver) testing must be conducted in a vacuum environment.

4.3.2 PCM Void Distributions. - Figure 8 shows radiographic images of typical PCM distributions within the canisters. The PCM void is generally comprised of a large primary cavity singly connected to one or more smaller secondary cavities. At room temperature, approximately 28 percent of the canister internal volume is void. The position and shape of the PCM void are markedly different in each test

expectations and with void distributions revealed in canister radiographs. These data demonstrate the ability of the PCM to stabilize local wall temperatures at slightly above the PCM melting point during the liquefication period (cycle time 6 to 45 min in figure 7). Similarly during PCM freezing (cycle time 60 to 72 min), local wall temperatures are essentially stabilized near the generally accepted PCM melting point of 1042 K. This so-called "thermal-arrest" behavior is most evident when the thermocouple is attached
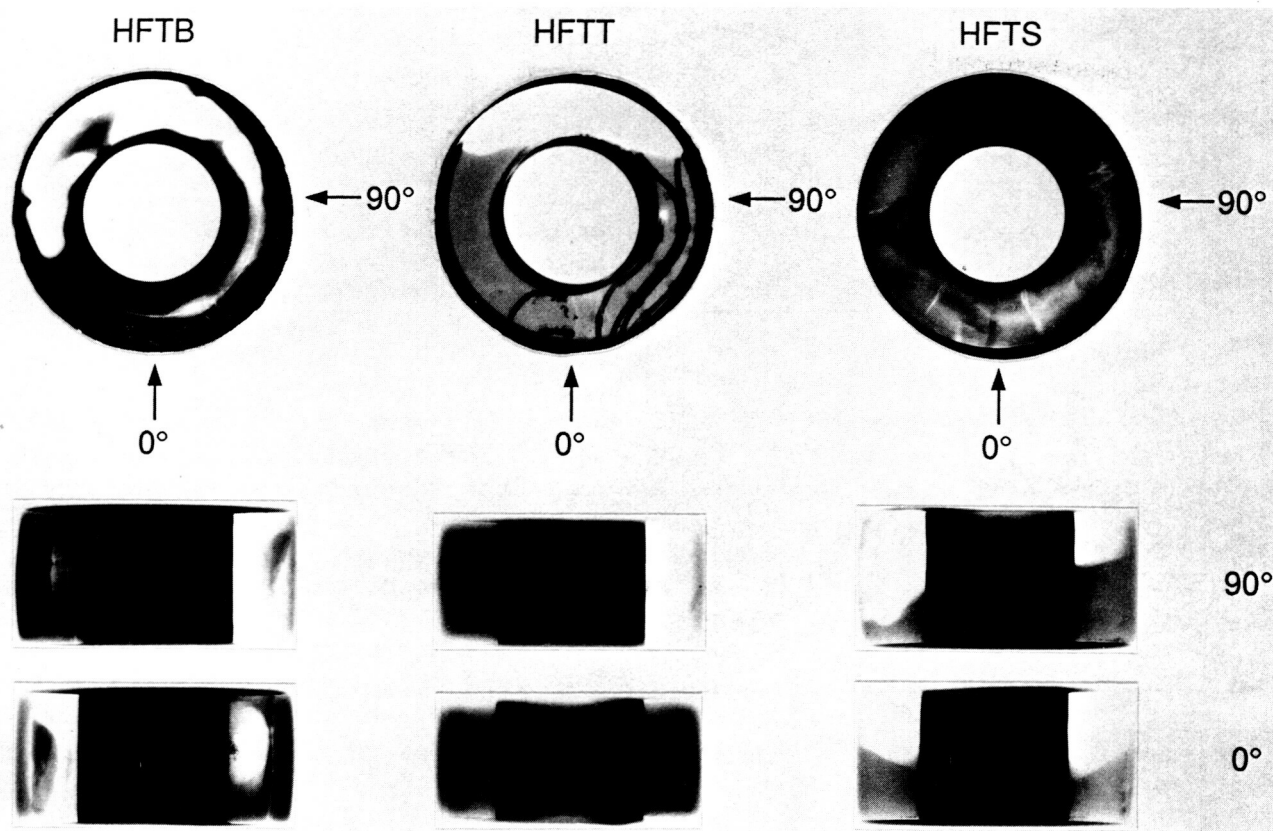
Figure 8.—Canister radiographs. Light regions indicate void; dark regions indicate PCM.

orientation. There appear to be three factors influencing the void distribution: (1) gravity, (2) canister heat removal, and (3) to a lesser extent, PCM wetting. In all orientations, the void is primarily located within the canister top volume as expected. However, the influence of canister heat removal is evident in the HFTB and HFTT orientations. In these tests, the direction of gravity was identical, yet the resulting void distributions were much different. This can be explained by the following observations concerning canister cooling.

For the first and only PCM freezing period in the HFTT orientation, the canister top region (facing the radiant heater) remained warmest. This resulted in PCM solidification that started from the lower, outer wall and proceeded radially inward and upward. Hence, liquid PCM was gravity-fed to fill solidification shrinkage and essentially all of the void formed in the canister uppermost volume. However, in the HFTB test, the canister bottom region (facing the radiant heater) remained warmest during the cooling period. This resulted in PCM·solidification that started from the upper portion of both inner and outer canister walls and proceeded downward. Hence, solidification shrinkage was not fed by liquid PCM and a crescent-shaped void, extending into the canister lower volume, formed at roughly the radial midpoint between outer and inner walls. These observations are consistent with those given in [2], [3], and [6].

A film of solid PCM also formed along the top canister surfaces in the HFTB and HFTS orientations (figure 8). This indicates that the liquid PCM has good wettability on HA 188 which allows a surface-tension flow of liquid PCM,

10

against gravity, to cover essentially all interior canister surface area. During micro-gravity canister operation, these surface-tension flows will undoubtedly have a larger relative influence on void shape and location than will buoyancy flows. Yet it remains clear that, regardless of the gravity environment, solidification will occur first at cooled boundaries in contact with liquid PCM (with the corollary that void volume will form at the warmest canister region(s)). Therefore, thermal boundary conditions will play a large role in determining void formation during 1-g and micro-g canister operation.

4.4 Evidence Of Liquid PCM Oscillatory Flow

At selected times during the 500 cycle HFTB test, a burst data collection mode was manually invoked to capture canister B outer wall temperature data (thermocouples 1, 2, 3, 10, and 11) at 2-sec intervals over a 10-min period. Figure 9 shows temperature data measured by thermocouples 1, 10, and 11
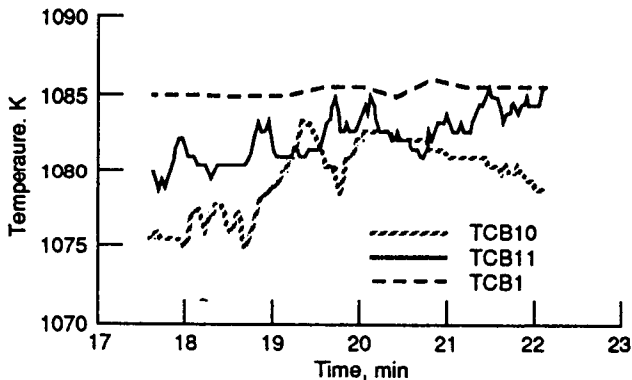

Figure 9.—Midstream canister temperature data for cycle 482 of the 500 cycle HFTB test.

over a 4 min period of cycle 482 which is also typical of other cycles. (Thermocouples 10 and 11 are attached to the outer wall at +45° and -45° around the canister circumference from thermocouple 1.) An alternating temperature response is evident for thermoocouples 10 and 11 while the response is nearly monotonic for thermocouple 1 over the same period. The response of thermocouples 2 and 3, not shown in figure 9, is also monotonic over this period of time. The alternating temperature response has approximately a 9-sec period which is close to the 10 to 20 sec period numerically predicted in [5]. In this work, flow field calculations showed that liquid PCM vortices would form and alternately rise up along each side of the canister outer wall during 1-g operation in the HFTB orientation. No alternating temperature responses were measured in the other 1-g test orientations.

While other causes for the alternating temperature responses cannot be totally ruled-out, the explanation of oscillatory flow in the melt seems the most plausible for the following reasons: (1) the alternating temperatures occurred at only the expected canister wall regions corresponding to the locations of thermocouples 10 and 11, (2) alternating temperatures were measured only during a finite portion of the cycle time, i.e., from approximately 9 to 23 min, while monotonic temperature response was measured for all other times, (3) the alternating temperature response was consistently measured for many separate cycles during the test, (4) the alternating temperature response occurred only when wall temperatures exceeded the PCM melting point, and (5) the period of measured wall temperature oscillation corresponds closely with the period of oscillating flow numerically predicted. Since the appropriate wall temperature predictions were not included in [4] or [5], the magnitude of expected wall temperature fluctuations is not known. These numerical predictions could help to further support (or refute) the premise of oscillating liquid PCM flow.

11

4.5 Comparison Of Experimental and Analytical Data

Figure 10 shows the comparison of analytical temperature predictions and experimental temperature data for cycle 10 of the first HFTS test (side wall thermocouples down). Refer to figure 5 for the locations of canister model finite-difference elements. The agreement between analytical and experimental temperatures is very good. The transition points between single and two-phase PCM, delineated by distinct temperature transient slope changes, are closely predicted throughout the cycle. Thermal-arrest wall temperature values are also closely predicted. Temperatures predicted generally fall within the temperature range measured by respective thermocouple pairs located 180° apart on the canister circumference (figure 10(a), TCB1 and TCB3 for example). Temperature differences from the canister front to back side are smallest at the side wall inner diameter (I.D.). As expected, the two-dimensional, axisymmetric canister computer model most accurately predicts temperatures (i.e., generally within ±5 K of TCB8 data) at this location.

A data feature not well captured by the computer model is the wall temperature transient associated with sensible PCM heating which starts at cycle times ranging from 20 to 50 min depending on canister location. During the period from 40 to 55 min, the computer model overpredicts canister side wall temperatures by 0 to 25 K. There are three possible explanations for this overprediction: (1) The axisymmetric computer model averages circumferential heat input to produce a symmetric PCM melt distribution. But heat input is not averaged during canister tests so that PCM melting must progress circumferentially around the canister from the hot side to the cold side. Hence, a longer time is required to fully melt the PCM in the experiment than was predicted and thus, experimental canister wall

temperatures were stabilized for a longer period of time. (2) The computer model ignores radiation heat transfer through the liquid PCM which is semi-transparent for wavelengths of interest. Lower canister wall temperatures would be predicted if this phenomenon was modeled. (3) The constant property, cooling air film coefficient used in the analysis might have led to an underprediction in canister convective cooling. This would result in a smaller predicted PCM melt time and higher canister wall temperatures than observed in the experiment.

Examination of the analytical results indicates that maximum wall temperatures during heating occur at the top of the outer wall adjacent to the void. PCM melting originates from the outer wall, starting at the PCM-void interface, and progresses radially inward, in a near-uniform fashion, along the length of PCM. Liquid PCM free convective effects are maximized shortly before complete melting occurs (at cycle time 39 min). At this time, local Nusselt numbers approach 9 which shows that significant convective heat transfer enhancement occurs during the latter portion of canister heating when operating in 1-g.

5 SUMMARY AND CONCLUDING REMARKS

Three PCM canisters were successfully tested for over 900 simulated Space Station Freedom orbital cycles. No canister cracks or leaks were observed at the conclusion of testing and all data were successfully collected. Some canister wall deformation occurred in two of the canisters. Stable and repeatable PCM properties were observed. The effect of 1-g test orientation on canister wall temperatures was generally small. However, the position and shape of the PCM void was strongly dependent on test orientation and the manner in which the canisters were cooled. The small differences in wall temperatures observed can be
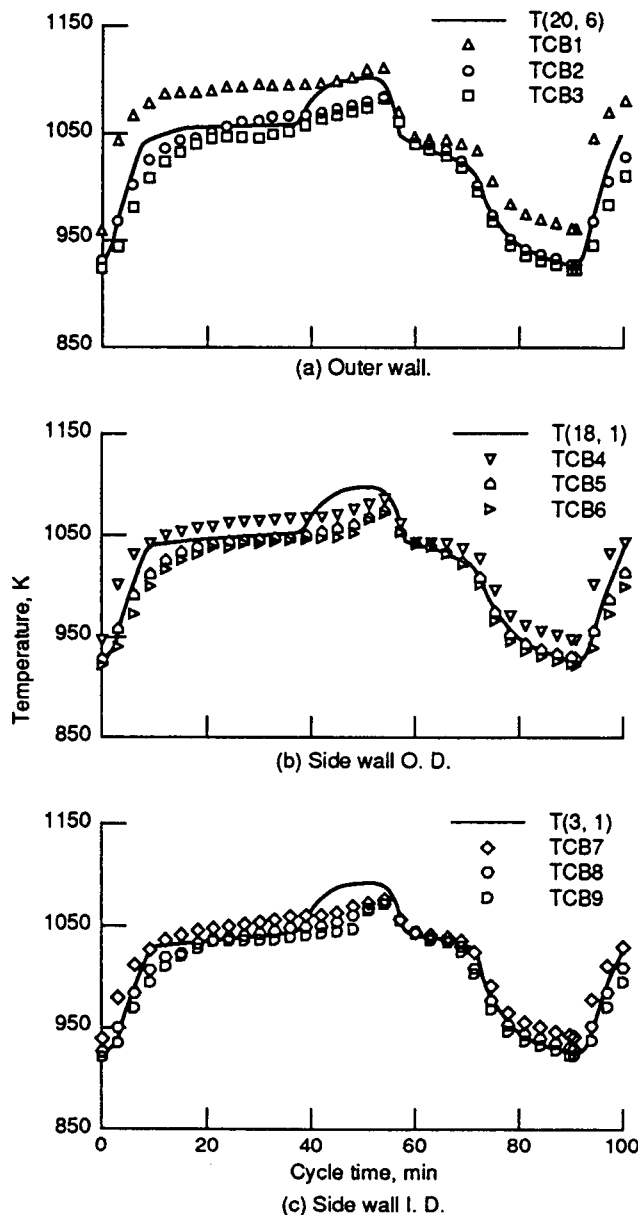
Figure 10.—Experimental versus analytical canister temperature data for cycle 10.

attributed to the magnitude of liquid PCM free convective flows and void location occurring in each different test orientation. Alternating wall temperature data, recorded in the HFTB test orientation, supports the theory of oscillating vortex flow in the PCM melt.

Analytical wall temperature predictions compared very favorably with canister temperature data. This illustrates that ground-based canister thermal performance can be predicted well by numerical canister analyses that employ straight-forward, engineering models of void behavior and liquid PCM free convection. Because 1-g canister heat transfer was accurately predicted and 1-g performance was relatively insensitive to test orientation (i.e., void location), canister performance in micro-g should be predicted with a high degree of confidence by removing gravity effects from the analytical modeling. A micro-g void location around the canister outer wall could be selected to assure conservative temperature predictions. Ground-based testing of receivers and canisters should be conducted with the axis-of-symmetry parallel to the gravity vector. This avoids introducing artificial circumferential temperature gradients and temperature transients from vortex flow in the melt which are not expected during micro-g operation.

ACKNOWLEDGEMENTS

REFERENCES

1. H.J. Strumpf, and M.G. Coombs, "Solar Receiver for the Space Station Brayton Engine," Transactions of the ASME, 87-GT-252, 1987.

2. J. Blumenberg, and S. Weingartner, "Preparation of a D2-Experiment for Analyzing the Thermal Properties of Relevant High-Temperature Storage Media Under Microgravity," IAF-88-211, 39th Congress of the International Astronautical Federation, Bangalore, India, October 8-15, 1988.

3. T.W. Kerslake, "Multi-Dimensional Modeling of a Thermal Energy Storage Canister," NASA TM-103731, January 1991.

4. R.P. Wichner, et al., "Thermal Analysis of Heat Storage Canisters for a Solar Dynamic, Space Power System," ORNL/TM-10665, 1988.

5. R.P. Wichner, et al., "Transient, Three-dimensional Analysis Of Thermal Energy Storage Phase Boundary and Void Behavior and Canister Stresses," Final Report DOE Interagency Agreement No. 1819-1819-A, July 1987.

6. H.J. Strumpf, and M.G. Coombs, "Solar Receiver Experiment for the Hybrid Space Station Brayton Engine," ASME Solar Energy Division Conference, San Diego, California, 1989.

7. K. Tanaka, et al., "Advanced Concepts for Latent Thermal Energy Storage for Solar Dynamic Receivers," Space Power, vol. 8, no. 4, pp. 425-434, 1989.

8. T.W. Kerslake, and M.B. Ibrahim, "Analysis of Thermal Energy Storage Material with Change-of-Phase Volumetric Effects," Proceedings of the 12th Annual ASME International Solar Energy Conference, ASME, New York, 1990, pp. 315-325. (see also, NASA TM-102457).

9. T.W. Kerslake, and M.B. Ibrahim, "Two-Dimensional Model of a Space Station Freedom Thermal Energy Storage Canister," Proceedings of the 25th Intersociety Energy Conversion Engineering Conference, vol. 2, 1990, pp 151-159. (see also, NASA TM-103124).

10. R. Siegel, and J.R. Howell, Thermal Radiation Heat Transfer: 2nd Edition, Hemisphere Publishing Corporation, 1981, pp. 243.

11. M.T. Tong, T.W. Kerslake, and R.L. Thompson, "Structural Assessment of a Space Station Solar Dynamic Heat Receiver Thermal Energy Storage Canister," Proceedings of the AIAA SDM Issues of the International Space Station Conference, Williamsburg Virginia, April 21-22, 1988, pp. 162-172.

NASA
National Aeronautics and
Space Administration

Report Documentation Page

1. Report No. NASA TM-104427	2. Government Accession No.	3. Recipient's Catalog No.

4. Title and Subtitle	5. Report Date
Experiments With Phase Change Thermal Energy Storage Canisters for Space Station Freedom	
	6. Performing Organization Code

7. Author(s)	8. Performing Organization Report No.
Thomas W. Kerslake	E-6102
	10. Work Unit No. 474-52-10

9. Performing Organization Name and Address	11. Contract or Grant No.
National Aeronautics and Space Administration Lewis Research Center Cleveland, Ohio 44135-3191	
	13. Type of Report and Period Covered

12. Sponsoring Agency Name and Address	Technical Memorandum
National Aeronautics and Space Administration Washington, D.C. 20546-0001	14. Sponsoring Agency Code

15. Supplementary Notes

16. Abstract

The solar dynamic power module proposed for the growth Space Station Freedom uses the heat of fusion of a phase change material (PCM) to efficiently store thermal energy for use during eclipse periods. The PCM, a $LiF-20CaF_2$ salt, is contained in annular, metal canisters located in a heat receiver at the focus of a solar concentrator. This paper discusses PCM canister ground-based experiments and analytical heat transfer studies. The hardware, test procedures, and test results from these experiments are discussed. After more than 900 simulated Space Station Freedom orbital cycles, no canister cracks or leaks were observed and all data were successfully collected. The effect of 1-g test orientation on canister wall temperatures was generally small while void position was strongly dependent on test orientation and canister cooling. In one test orientation, alternating wall temperature data were measured that supports an earlier theory of oscillating vortex flow in the PCM melt. Analytical canister wall temperatures compared very favorably with experimental temperature data. This illustrates that ground-based canister thermal performance can be predicted well by analyses that employ straight-forward, engineering models of void behavior and liquid PCM free convection. Because of the accuracy of analytical models and the relative insensitivity of 1-g performance to test orientation, canister performance in micro-g should be predictable with a high degree of confidence by removing gravity effects from the analytical modeling.

17. Key Words (Suggested by Author(s))	18. Distribution Statement
Space stations; Solar dynamic power systems; Phase change materials; Heat storage; Experimentation; Gravitational effects; Voids	Unclassified - Unlimited Subject Category 20

19. Security Classif. (of the report)	20. Security Classif. (of this page)	21. No. of pages	22. Price*
Unclassified	Unclassified	16	A03